Ann. Acad. Rom. Sci.
Ser. Math. Appl.
ISSN 2066-6594 Vol. 17, No. 3/2025

ADVANCED MODEL FOR OPTIMAL MANAGEMENT OF ENERGY DEFICITS AND SURPLUSES IN STAND-ALONE DIRECT-CURRENT MICROGRIDS*

Annunziata Palumbo† Mario Versaci‡

Dedicated to Prof. Liliana Restuccia on the occasion of her 70th anniversary

DOI 10.56082/annalsarscimath.2025.3.133

Abstract

This work presents an energy management system for stand-alone direct current microgrids, based on a fuzzy controller that employs a bracket operator. The system takes as input the net power and the state of charge of the storage unit, processed through a structure inspired by proportional-integral-derivative regulators. The control logic effectively governs the activation of the fuel cell, optimizing resource usage while maintaining operational stability. The performance of the system, validated on both simulated and real data, shows a high degree of consistency in the two contexts, confirming the reliability of the approach and the potential of simulation as a support tool for designing real-world systems with a low error margin.

Keywords: microgrid control, fuzzy bracket controller, PID-inspired fuzzy logic, intelligent energy management system.

MSC: 93A30, 93C42, 68T27, 90B30.

*Accepted for publication on September 22, 2025

†apalumbo@unime.it, MIFT Department, University of Messina, Viale F. d'Alcontres 31, I-98166, Messina, Italy

‡mario.versaci@unirc.it, DICEAM Department, Mediterranea University, Via Zehender (ex Via Graziella Feo di Vito), I-89122 Reggio Calabria, Italy

1 Introduction

Standalone direct current microgrids (Stand-alone DC-MG) are emerging as an efficient and flexible solution for energy supply in remote areas, isolated communities, and emergency scenarios [14, 16, 18, 19]. They allow the direct integration of renewable energy sources (RES), such as photovoltaic and wind power, with storage systems and local loads, offering advantages over alternative current (AC) grids, including higher efficiency, reduced losses, and simplified management of electronic devices [4, 18]. The absence of connection to the main grid requires advanced local control to ensure operational continuity and stability [3, 12, 17]. In this context, the generated energy is regulated by power electronic converters and directed toward the loads or batteries, typically lead-acid types [11, 15]. In cases of production shortfall, a fuel cell (FC) ensures continuous power supply. The energy management system plays a central role, balancing supply and demand in real time, optimizing resource usage, and regulating the state of charge [15, 19]. However, managing these microgrids still presents challenges due to the variability of RES and loads, which demand intelligent and adaptive energy management systems (EMS) capable of operating under uncertainty [6, 8]. Deterministic controllers, though accurate, are often unsuitable for real-time control due to their high computational load [9]. Proportional–integral–derivative (PID) regulators, while simple, fail to effectively manage nonlinearities and variability [13]. Other approaches, such as hierarchical control and metaheuristics, introduce additional complexity and response times that are often incompatible with operational requirements [10]. In this scenario, fuzzy controllers offer a valuable alternative due to their ability to handle uncertainty without requiring rigorous mathematical models [19]. However, classical Mamdani and Sugeno models are limited in representing time-varying dynamics, while intuitionistic fuzzy systems and deep-fuzzy architectures, despite improving response under complex conditions, significantly increase design and computational complexity [12, 16, 17, 18, 19]. Experiences with Mamdani-type fuzzy EMS in hardware-in-the-loop configurations show promising results in maintaining stability and regulating the battery state of charge (%SoC), but the rigidity of rule sets and lack of dynamic modeling limit their effectiveness in highly variable scenarios [7]. These considerations highlight the need for a more solid framework to model the dynamic interactions between interdependent variables. Conventional approaches fail to guarantee fundamental properties such as antisymmetry, nilpotency, and internal coherence, compromising the balance between robustness, accuracy, and efficiency [2].

The study proposes an innovative approach to energy management in standalone DC microgrids, based on a fuzzy structure that synergistically integrates the fuzzy bracket formalism with the logic of PID controllers. This combination overcomes the limitations of traditional fuzzy controllers by introducing a structured and mathematically consistent mechanism to represent temporal dynamics and nonlinear relationships between variables. The fuzzy bracket goes beyond the conventional role of modeling relationships among linguistic variables, embedding an operational logic analogous to that of PID controllers, thereby enabling a continuous representation of proportional, integral, and derivative effects. Unlike Lie algebras, which emphasize formal constraints such as the Jacobi identity, the fuzzy algebra employed here is grounded in functional coherence among system elements, favoring practical effectiveness over structural rigidity. This synergy between the fuzzy bracket and PID logic endows the energy management system with adaptive, stable, and highly responsive behavior. The resulting EMS manages net power and battery state of charge (%SoC) in real time, precisely modulating fuel cell activation and ensuring optimal energy balance even under significant fluctuations in generation and load. The results, confirmed through simulations and validated against real data, demonstrate the robustness and effectiveness of this architecture, which combines mathematical rigor, engineering interpretability, and low computational cost. As such, the proposed framework represents a significant contribution to the advancement of fuzzy systems for advanced energy applications, offering a solid theoretical and practical foundation for the development of next-generation autonomous microgrids.

The paper is structured as follows. Section 2 describes the considered microgrid, while Section 3 introduces the architecture of the energy management system. Section 4 defines the fuzzy bracket operator, and Section 5 presents the fuzzification inspired by PID controllers. In Section 6, the complete fuzzy controller is illustrated. Sections 7 and 8 focus respectively on the management of the fuel cell and the damp load. Sections 9 and 10 analyze simulated and real data, and Section 11 compares the corresponding results. Section 12 provides a comparative analysis, followed by conclusions and future perspectives in Section 13.

2 DC microgrid model

The stand-alone DC-MG here studied is an isolated direct current network designed to ensure energy autonomy in the absence of a connection to the main grid. It integrates variable renewable energy sources (photovoltaic and wind), a lead-acid battery storage system to stabilize the network, a hydrogen fuel cell (FC) that activates during energy shortages, and a damp load to handle energy surpluses. The flow management is entrusted to an intelligent system that balances production and consumption in real time, ensuring operational continuity, efficiency, and reliability.

2.1 PV and WT systems

The photovoltaic (PV) system consists of a number of panels connected to the DC bus via a DC/DC boost converter. The output power, $P_{PV}(t)$ (W), can be evaluated using the well-known relation [4, 19]:

$$P_{PV}(t) = P_{PV rated}\frac{G_t(t)}{1000}\Big\{1 + \alpha_t\Big[T_{amb} + 0.0256G_t(t)\Big] - T_{C_{STC}}\Big\}, \qquad (1)$$

where $G_t(t)$ is the solar irradiance (W/m^2); $P_{PV rated}$ is the rated power[1] (W) of the PV module under standard test conditions (STC), and $\alpha_t = -3.7\times10^{-3}$ $(°\mathrm{C})^{-1}$ denotes the temperature coefficient. Finally, $T_{C_{STC}}$ is the cell temperature (°C) under STC, and T_{amb} is the ambient temperature (°C). We employ a permanent magnet synchronous generator directly coupled to the wind turbine (WT), which always operates below its rated speed[2]. The mechanical power generated is quantified as follows [16]:

$$P_{mechanical}(t) = 0.5\rho\pi R^2(v(t))^3 C_p(\lambda, \beta), \qquad (2)$$

where ρ is the air density (kg/m^3), R is the blade radius (m), $v(t)$ is the wind speed (m/s), and $C_p(\lambda, \beta)$ is the power coefficient of the WT, which expresses the relationship between the tip-speed ratio (λ) and the pitch angle (β). Typically, $C_p(\lambda, \beta) = 0.593$ is used (Betz limit).

2.2 Battery model and state of charge

The lead-acid battery model takes into account the charge/discharge dynamics, nominal capacity, and voltage and current limits, storing excess energy from the RES and releasing it during deficit periods. The state of charge

[1] Maximum continuous power allowed without causing overheating or damage.

[2] Rotor speed at which a wind turbine delivers its maximum continuous power without overheating or sustaining damage.

$SoC(t)$, defined as the fraction of available energy relative to the maximum capacity, is given by [16, 19]:

$$SoC(t) = SoC(0) - \frac{1}{C_{\text{batt}}} \int_0^t I_{\text{batt}}(\tau)\, d\tau, \tag{3}$$

where C_{batt} is the nominal capacity (Ah), and $I_{\text{batt}}(t)$ is the battery current (positive during discharge, negative during charge). In advanced models, the SoC is normalized within the interval [0,1] and can be expressed in fuzzy form to optimize energy management via the EMS. The model also accounts for nonlinear phenomena such as internal resistance, charge efficiency, and cycle degradation, which are essential for reliable long-term performance forecasting.

2.3 Fuel cell

We use a proton exchange membrane fuel cell (PEMFC), in line with the Tech4You project, which converts chemical energy into electrical energy through the reaction between H_2 and O_2, producing electricity, water, and heat. Hydrogen is oxidized at the anode, while oxygen accepts electrons at the cathode, with the electron flow passing externally through the circuit. The ideal open-circuit voltage E_{OC} (V) depends on the Gibbs free energy and is calculated as follows [18, 19]:

$$E_{OC} = K_C \left[E_C + (T - 298)\frac{-44.43}{zF} + \frac{RT}{zF} \ln\left(P_{H_2} \sqrt{P_{O_2}} \right) \right]. \tag{4}$$

The term E_{OC} represents the ideal open-circuit voltage and is expressed in volts [V]. The coefficient K_C is dimensionless and serves as an empirical correction factor. The value E_C, also in volts [V], represents the standard voltage associated with the redox reaction between hydrogen and oxygen under standard conditions. The temperature T is expressed in kelvin [K], while the constant -44.43 represents the derivative of the Gibbs free energy with respect to temperature, with units of kilojoules per mole [kJ/mol]. The parameter z is dimensionless and indicates the number of electrons transferred per mole of reaction, while F is the Faraday constant, expressed in coulombs per mole [C/mol]. The universal gas constant R is expressed in joules per mole per kelvin [J/(mol·K)], and together with the temperature T, it enters the Nernst correction through the term $\frac{RT}{zF} \ln\left(P_{H_2}\sqrt{P_{O_2}}\right)$, which ultimately yields a voltage in volts [V]. The partial pressures of hydrogen P_{H_2} and oxygen P_{O_2} are expressed in atmospheres [atm] or bars, and their logarithmic contribution is dimensionless. Overall, the entire expression within square brackets is in volts [V], maintaining the dimensional consistency of the formula. Under real operating conditions, the voltage is reduced by two main losses. The first is the activation loss U_{act}, due to catalytic phenomena:

$$U_{act} = \frac{NA_{nom}}{\tau_s + 1} \ln\left(\frac{i_{fc}}{i_0}\right). \tag{5}$$

The term U_{act} represents the activation voltage loss and is expressed in volts [V]. The coefficient N is dimensionless and indicates the number of cells in the fuel cell stack. The parameter A_{nom} is an empirical coefficient related to the nominal current density and catalytic effects, with units of volts [V]. The term τ_s is a dimensionless parameter representing a delay effect associated with the system dynamics. The ratio $\frac{i_{fc}}{i_0}$ is dimensionless, where i_{fc} is the instantaneous current delivered by the fuel cell, measured in amperes [A], and i_0 is the exchange current, also in amperes [A]. The natural logarithm of this ratio yields a dimensionless quantity. Overall, the expression results in a voltage value in volts [V], consistent with the unit of U_{act}. The second is the ohmic loss U_{ohmic}, caused by the internal resistance of the stack, expressed as $U_{ohmic} = R_{in}\, i_{fc}$. Therefore, the actual cell voltage is given by $U_{cell} = E_{OC} - U_{act} - U_{ohmic}$.

2.4 Load and net power definition

The loads represent the power demand from local users and include all devices and equipment powered by the system. The available power, on the other hand, primarily comes from renewable energy sources (RES), whose production is subject to variability. To evaluate the energy balance, we introduce the net power $P_{\text{net}}(t)$, defined as the difference between the power required by the loads $P_{\text{load}}(t)$ and the sum of the power generated by the renewable sources $P_{\text{RES}}(t)$ (or vice versa, depending on the adopted convention) [19], $P_{\text{net}}(t) = P_{\text{load}}(t) - P_{\text{RES}}(t)$, where $P_{\text{RES}}(t) = P_{\text{PV}}(t) + P_{\text{WT}}(t)$. If $P_{\text{net}}(t) > 0$, the power demand is not fully covered by RES and the deficit must be compensated by the battery or the fuel cell (FC). If $P_{\text{net}}(t) < 0$, there is an energy surplus that can be stored in the battery system.

3 EMS of the stand-alone DC-MG

The Energy Management System (EMS) aims to maintain, in real time, the balance among the power generated by renewable energy sources (RES), the available storage capacity, and the load demand in an islanded DC micro-grid. The diagram shown in Fig. 1 depicts exactly the architecture adopted in this work, with the acquisition/normalization, fuzzification, inference, and defuzzification blocks that generate the power reference for the fuel cell (FC). The controller is based on fuzzy logic and is designed for scenarios with high variability and uncertainty. It has two inputs: (i) the net power—defined as the difference between load demand and RES generation—which instantaneously measures surpluses or deficits; and (ii) the battery state-of-charge percentage (%SoC), indicative of the residual capability to store/release energy. Both quantities are mapped into linguistic variables via membership functions, avoiding hard thresholds and enabling smooth transitions between conditions such as "surplus/deficit" and "low/medium/high battery." The inference engine combines evidence from net power and %SoC and determines the contribution to assign to the FC. The EMS output is therefore a power set-point (or modulation command) indicating how much power the FC should deliver or curtail to compensate for any imbalances. Fuzzy logic enables dynamic adaptation: in case of surplus the FC remains off; in the presence of a deficit it is progressively activated; and during fast transients in load or generation the response is prompt and consistent, preserving bus stability and avoiding unnecessary activations. All this occurs while respecting device operating constraints (power limits and storage operating windows). From an architectural standpoint, the processing flow (the one actually employed in this study, as shown in Fig. 1) comprises: (i) signal pre-processing and normalization; (ii) input fuzzification according to calibrated linguistic sets; (iii) a rule base of the "IF... THEN..." type that maps combinations of "deficit/surplus" and "low/medium/high SoC" into FC support levels; and (iv) defuzzification that yields a single, consistent set-point to be sent to the power converters. The chain is computationally light and supports continuous set-point updates, prioritizing efficient use of storage and limiting FC intervention to what is necessary, thus reducing consumption and wear.

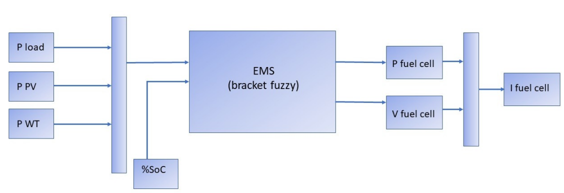

Figure 1: The EMS, structured through a bracket-based fuzzy control, uses net power and the battery's %SoC as inputs.

4 Bracket fuzzy approach

This section presents the fuzzy bracket, the core of the controller: a binary operation on fuzzy variables that encodes the interaction between net power and state of charge, providing a coherent measure of energy imbalance. Its algebra is defined by two key properties, antisymmetry and nilpotency, ensuring balanced responses to surplus and deficit while avoiding unnecessary actions at equilibrium.

4.1 Fuzzy algebra and bracket

A fuzzy algebra $(\mathcal{F}, [\cdot,\cdot]_\mu)$ is a fuzzy algebraic structure consisting of a set $\mathcal{F}$ of fuzzy membership functions and a binary operation $[\cdot,\cdot]_\mu$, called the fuzzy bracket, which describes relationships and interactions among fuzzy elements $\mu_1, ...\mu_i, ..., \mu_n \in \mathcal{F}$, where each μ_i represents a fuzzy function mapping a given variable into the interval $[0, 1]$. The operation $[\cdot,\cdot]_\mu$ is designed to satisfy two fundamental properties: *antisymmetry* and *nilpotency*, which are essential for ensuring mathematical consistency, robustness, and adaptability to the complex dynamics of an EMS. Antisymmetry implies that swapping the arguments in the bracket reverses the sign of the expression:

$$[\mu_1, \mu_2]_\mu = -[\mu_2, \mu_1]_\mu, \quad \forall \mu_1, \mu_2 \in \mathcal{F}. \tag{6}$$

This property reflects a consistent bilateral relationship between fuzzy variables, ensuring a complementary response in opposing scenarios, such as energy surplus and deficit, and preventing contradictions in control. In an EMS, this allows symmetric handling of conditions like overload and underload, ensuring consistent resource management. Nilpotency, on the other hand, states that the bracket between two identical variables is zero:

$$[\mu_s, \mu_s]_\mu = 0, \quad \forall \mu_s \in \mathcal{F}. \tag{7}$$

This property prevents unnecessary reactions under balanced conditions, promoting energy savings and control stability. When net power and state of charge are balanced, the system avoids activating auxiliary sources such as the FC. Nilpotency also helps reduce numerical noise, increase robustness in uncertain environments, and prevent logical conflicts, ensuring consistency even during rapid fluctuations. Together, antisymmetry and nilpotency enable the fuzzy bracket to describe both instantaneous variations and operational memory, providing a reliable foundation for intelligent and efficient control in stand-alone DC-MG.

5 Bracket fuzzy formulation

An effective formulation of the fuzzy bracket must robustly represent energy balance under complex operating conditions, adapting to dynamic changes. In this context, the EMS must continuously compare energy demand and supply, considering intermittent RES and storage systems. It is worth noting that he comparison between $\mu(P_{net}(t))$ and $\mu(SoC(t))$ is expressed as $\mu(P_{net}(t))-\mu(SoC(t))$: positive values indicate an energy deficit that should be compensated by auxiliary resources, while negative values reflect remaining battery capacity useful for absorbing excess energy. By these premises, we introduce the following definition.

Definition 1 (Bracket fuzzy for EMS)

$$[\mu(P_{net}(t)), \mu(SoC(t))]_\mu = \frac{\mu(P_{net}(t)) - \mu(SoC(t))}{1 + |\mu(P_{net}(t))| + |\mu(SoC(t))|}. \tag{8}$$

This formulation provides a dimensionless and normalized measure of the instantaneous energy imbalance between net power and storage state, ensuring antisymmetry and nilpotency while preventing excessive sensitivity to extreme operating conditions. It serves as a coherent indicator for the EMS to decide whether to activate auxiliary sources or manage surplus energy.

The term $1 + |\mu(P_{net}(t))| + |\mu(SoC(t))|$ in (8) stabilizes the fuzzy bracket value by scaling $\mu(P_{net}(t)) - \mu(SoC(t))$ to avoid undesired amplification. Unlike classical normalization, $1 + |\mu(P_{net}(t))| + |\mu(SoC(t))|$ can exceed 1, reducing sensitivity to extreme variations and ensuring consistency even under critical operating conditions.[3] Physically, equation (8) provides a balanced measure of the deviation between the instantaneous energy demand, described by $\mu(P_{\text{net}}(t))$, and the storage or release capacity, represented by $\mu(\text{SoC}(t))$. Thanks to the sign of the result, the EMS can quickly determine whether it needs to compensate for an energy deficit (by activating the fuel cell) or manage a surplus (by charging the battery or reducing generation).

Remark 1 (8) *expresses the relationship between $P_{net}(t)$ and the battery state of charge* SoC(t)*. The FC power $P_{FC}(t)$ is not derived directly from the bracket, but from fuzzy rules based on these variables (see below). This separation simplifies the model, preserves structural properties such as antisymmetry, and ensures logical consistency by providing predictable responses*

[3] Unlike classical normalization based on fixed constants or maxima within [0,1], the denominator here adapts dynamically to the system state and can exceed 1.

to input changes. As a result, the EMS ensures stable, adaptive control and optimizes energy management based on the dynamics of $P_{net}(t)$ and $\mathrm{SoC}(t)$.

The following results yield.

Proposition 1 *The bracket* (8) *is antisymmetric and nilpotent.*

Proof. Swapping the arguments in (8) yields:

$$[\mu(SoC(t)), \mu(P_{\text{net}}(t))]_\mu = -[\mu(P_{\text{net}}(t)), \mu(SoC(t))]_\mu. \tag{9}$$

In other words, inverting the variables produces an opposite response, allowing the distinction between a deficit ($P_{\text{net}}(t) > 0$), where demand exceeds supply or storage, and a surplus ($P_{\text{net}}(t) < 0$), where available energy exceeds demand. If the two arguments coincide, that is, $\mu(P_{\text{net}}(t)) = \mu(\mathrm{SoC}(t)) = \mu_0$, we obtain $[\mu_0, \mu_0]_\mu = \frac{\mu_0 - \mu_0}{1+|\mu_0|+|\mu_0|} = 0$. The nilpotency of (8) is essential for the EMS, as a zero value—when net power and state of charge coincide—indicates an energy balance condition: the system avoids unnecessary control actions, activating resources only in the presence of actual imbalances, with benefits in terms of coherence, stability, and operational efficiency.

Proposition 2 *The denominator in* (8) *acts as a normalizing factor.*

Proof. Denoting $\mu_1 = \mu(P_{\text{net}}(t))$ and $\mu_2 = \mu(\mathrm{SoC}(t))$, we consider:

$$-1 < |[\mu_1, \mu_2]_\mu| = \left| \frac{\mu_1 - \mu_2}{1 + |\mu_1| + |\mu_2|} \right| \leq \frac{|\mu_1| + |\mu_2|}{1 + |\mu_1| + |\mu_2|} < 1. \tag{10}$$

In engineering applications, the Jacobi identity is unnecessary because the fuzzy bracket is used only on pairs of variables, not in nested operations. The properties of antisymmetry and nilpotency are sufficient to ensure consistency and control stability, avoiding unnecessary complexity and making the system simple, efficient, and suitable for real-time implementation.

6 SPID-inspired structure and innovative membership functions

The integration of the PID structure with (8) merges fuzzy logic flexibility with PID responsiveness, enabling robust, adaptive control that handles uncertainty and maintains energy balance under variable conditions. To enhance the EMS, the membership functions $\mu(P_{\mathrm{net}}(t))$ and $\mu(\mathrm{SoC}(t))$ follow a PID-based design, incorporating past, present, and predictive information through proportional, integral, and derivative components, respectively.

6.1 Design of membership functions

As expected for PID systems, we define $\mu(P_{\mathrm{net}}(t))$ as follows [1, 5]:

$$\mu(P_{\mathrm{net}}(t)) = \alpha(t) \int_0^t P_{\mathrm{net}}(\tau)\, d\tau + \beta(t) P_{\mathrm{net}}(t) + \gamma(t) \frac{d}{dt} P_{\mathrm{net}}(t), \tag{11}$$

whose dynamic parameters are [5] $\alpha(t) = \alpha_0 + k_\alpha \int_0^t P_{\mathrm{net}}(\tau)\, d\tau$, $\beta(t) = \beta_0 + k_\beta P_{\mathrm{net}}(t)$ and $\gamma(t) = \gamma_0 + k_\gamma \frac{d}{dt} P_{\mathrm{net}}(t)$. By substituting these parameters into (11), we obtain:

$$\begin{aligned} \mu(P_{\mathrm{net}}(t)) = \alpha_0 \int_0^t P_{\mathrm{net}}(\tau)\, d\tau + k_\alpha \left(\int_0^t P_{\mathrm{net}}(\tau)\, d\tau \right)^2 + \\ + \beta_0 P_{\mathrm{net}}(t) + k_\beta \left(P_{\mathrm{net}}(t) \right)^2 + \gamma_0 \frac{d}{dt} P_{\mathrm{net}}(t) + k_\gamma \left(\frac{d}{dt} P_{\mathrm{net}}(t) \right)^2. \end{aligned} \tag{12}$$

To ensure that $\mu(P_{\mathrm{net}}(t)) \in [0, 1]$, each term is normalized based on its theoretical maximum value. Considering the first term, since $P_{\max}$ is the expected maximum value of $P_{\mathrm{net}}(t)$, we have $\int_0^t P_{\mathrm{net}}(\tau)\, d\tau \leq t P_{\max}$, from which it follows that

$$\alpha_0 = \frac{\alpha_0'}{t P_{\max}}, \quad \alpha_0' \in [0, 1]. \tag{13}$$

Regarding the second term, noting that $\left(\int_0^t P_{\mathrm{net}}(\tau)\, d\tau \right)^2 \leq (t \cdot P_{\max})^2$, we obtain

$$k_\alpha = \frac{k_\alpha'}{(t P_{\max})^2}, \quad k_\alpha' \in [0, 1]. \tag{14}$$

Similarly, the third and fourth terms yield:

$$\beta_0 = \frac{\beta_0'}{P_{\max}}, \quad \beta_0' \in [0, 1], \qquad k_\beta = \frac{k_\beta'}{P_{\max}^2}, \quad k_\beta' \in [0, 1], \tag{15}$$

respectively. The fifth term, $\gamma_0 \frac{d}{dt} P_{\mathrm{net}}(t)$, since the derivative is bounded within $[\dot{P}_{\min}, \dot{P}_{\max}]$, leads to the following normalization of γ_0:

$$\gamma_0 = \frac{\gamma_0'}{\dot{P}_{\max}}, \quad \gamma_0' \in [0, 1]. \tag{16}$$

likewise, the sixth term normalizes k_γ as follows:

$$k_\gamma = \frac{k'_\gamma}{\dot{P}^2_{\max}}, \quad k'_\gamma \in [0,1]. \tag{17}$$

By substituting the normalized parameters into equation (12), we obtain: the new version of $\mu(P_{\text{net}}(t))$:

$$\begin{aligned} \mu(P_{\text{net}}(t)) = \\ = \frac{\alpha'_0}{t \cdot P_{\max}} \int_0^t P_{\text{net}}(\tau)\, d\tau + \frac{k'_\alpha}{(t \cdot P_{\max})^2} \left(\int_0^t P_{\text{net}}(\tau)\, d\tau \right)^2 + \\ + \frac{\beta'_0}{P_{\max}} P_{\text{net}}(t) + \frac{k'_\beta}{P^2_{\max}} (P_{\text{net}}(t))^2 + \\ + \frac{\gamma'_0}{\dot{P}_{\max}} \frac{d}{dt} P_{\text{net}}(t) + \frac{k'_\gamma}{\dot{P}^2_{\max}} \left(\frac{d}{dt} P_{\text{net}}(t) \right)^2. \end{aligned} \tag{18}$$

Since the sum of the terms cannot exceed 1, we introduce a normalization factor $N_P = \alpha'_0 + k'_\alpha + \beta'_0 + k'_\beta + \gamma'_0 + k'_\gamma$, the updated version of (18) becomes:

$$\begin{aligned} \mu(P_{\text{net}}(t)) = \frac{1}{N_P} \Bigg(\frac{\alpha'_0}{t \cdot P_{\max}} \int_0^t P_{\text{net}}(\tau)\, d\tau + \\ + \frac{k'_\alpha}{(t \cdot P_{\max})^2} \left(\int_0^t P_{\text{net}}(\tau)\, d\tau \right)^2 + \frac{\beta'_0}{P_{\max}} P_{\text{net}}(t) + \frac{k'_\beta}{P^2_{\max}} (P_{\text{net}}(t))^2 + \\ + \frac{\gamma'_0}{\dot{P}_{\max}} \frac{d}{dt} P_{\text{net}}(t) + \frac{k'_\gamma}{\dot{P}^2_{\max}} \left(\frac{d}{dt} P_{\text{net}}(t) \right)^2 \Bigg), \end{aligned} \tag{19}$$

ensuring that $0 \leq \mu(P_{\text{net}}(t)) \leq 1$.
As for $\mu(P_{\text{net}}(t))$, we define $\mu(\text{SoC}(t))$ as follows [5]:

$$\mu(SoC(t)) = \lambda(t) SoC(t) + \delta(t) \frac{d}{dt} SoC(t) + \eta(t) \int_0^t SoC(\tau)\, d\tau, \tag{20}$$

where the dynamic parameters $\lambda(t)$, $\delta(t)$, and $\eta(t)$ are expressed as:

$$\begin{aligned} \lambda(t) = \lambda_0 + k_\lambda SoC(t), \\ \delta(t) = \delta_0 + k_\delta \frac{d}{dt} SoC(t), \quad \eta(t) = \eta_0 + k_\eta \int_0^t SoC(\tau)\, d\tau. \end{aligned} \tag{21}$$

By substituting these parameters, the new version of (20) becomes:

$$
\begin{aligned}
&\mu(SoC(t)) = \\
&= \lambda_0 SoC(t) + k_\lambda \left(SoC(t)\right)^2 + \delta_0 \frac{d}{dt} SoC(t) + \\
&+ k_\delta \left(\frac{d}{dt} SoC(t)\right)^2 + \eta_0 \int_0^t SoC(\tau)\, d\tau + k_\eta \left(\int_0^t SoC(\tau)\, d\tau\right)^2 .
\end{aligned}
\tag{22}
$$

To ensure that $\mu(\mathrm{SoC}(t)) \in [0,1]$, each term is normalized as follows. In $\lambda_0\,\mathrm{SoC}(t)$, since $\mathrm{SoC}(t) \in [0,1]$, we normalize λ_0 as $\lambda_0 = \lambda'_0 \in [0,1]$. The second term, $k_\lambda\,(\mathrm{SoC}(t))^2$, has a maximum value of 1, so we set $k_\lambda = k'_\lambda \in [0,1]$. For the term $\delta_0 \frac{d}{dt}\mathrm{SoC}(t)$, since $\frac{d}{dt}\mathrm{SoC}(t) \in [\dot{\mathrm{SoC}}_{\min}, \dot{\mathrm{SoC}}_{\max}]$, we normalize as $\delta_0 = \frac{\delta'_0}{\dot{\mathrm{SoC}}_{\max}}, \quad \delta'_0 \in [0,1]$. The term $k_\delta \left(\frac{d}{dt}\mathrm{SoC}(t)\right)^2$ reaches a maximum value of $\dot{\mathrm{SoC}}^2_{\max}$, so we normalize it as $k_\delta = \frac{k'_\delta}{\dot{\mathrm{SoC}}^2_{\max}}, \quad k'_\delta \in [0,1]$. For the fifth term, $\eta_0 \int_0^t \mathrm{SoC}(\tau)\, d\tau$, given that the theoretical maximum of the integral is t, we set $\eta_0 = \frac{\eta'_0}{t}, \quad \eta'_0 \in [0,1]$. The sixth term, $k_\eta \left(\int_0^t \mathrm{SoC}(\tau)\, d\tau\right)^2$, has a maximum value of t^2, and is normalized as $k_\eta = \frac{k'_\eta}{t^2}, \quad k'_\eta \in [0,1]$. By substituting the normalized parameters into (22), the new version of $\mu(SoC(t))$ becomes:

$$
\begin{aligned}
\mu(SoC(t)) = \lambda'_0 SoC(t) + k'_\lambda \left(SoC(t)\right)^2 + \frac{\delta'_0}{\dot{SoC}_{\max}} \frac{d}{dt} SoC(t) + \\
+ \frac{k'_\delta}{\dot{SoC}^2_{\max}} \left(\frac{d}{dt} SoC(t)\right)^2 + \\
+ \frac{\eta'_0}{t} \int_0^t SoC(\tau)\, d\tau + \frac{k'_\eta}{t^2} \left(\int_0^t SoC(\tau)\, d\tau\right)^2 .
\end{aligned}
\tag{23}
$$

Since the sum of the terms may exceed 1, we introduce a normalization factor $N = \lambda'_0 + k'_\lambda + \delta'_0 + k'_\delta + \eta'_0 + k'_\eta$, so that

$$
\begin{aligned}
\mu(SoC(t)) = \frac{1}{N} \Bigg(\lambda'_0\, SoC(t) + k'_\lambda \left(SoC(t)\right)^2 + \frac{\delta'_0}{\dot{SoC}_{\max}} \frac{d}{dt} SoC(t) \\
+ \frac{k'_\delta}{(\dot{SoC}_{\max})^2} \left(\frac{d}{dt} SoC(t)\right)^2 + \\
+ \frac{\eta'_0}{t} \int_0^t SoC(\tau)\, d\tau + \frac{k'_\eta}{t^2} \left(\int_0^t SoC(\tau)\, d\tau\right)^2 \Bigg),
\end{aligned}
\tag{24}
$$

ensuring that $0 \leq \mu(\mathrm{SoC}(t)) \leq 1$. Incorporating temporal dynamics into $\mu(P_{\mathrm{net}}(t))$ and $\mu(\mathrm{SoC}(t))$ allows the energy management system to integrate both instantaneous and cumulative information, resulting in more consistent control. Parameters (11) and (21) adaptively tune the proportional, integral, and derivative contributions: the integral term compensates for long-lasting imbalances and dampens oscillations, while the derivative term detects rapid changes in $\%SoC$ and triggers timely responses.

Remark 2 *The quadratic terms in* (12) *and* (22) *model the nonlinearities of $P_{net}(t)$ and $SoC(t)$, highlighting large variations under overloads or deep discharges and capturing effects such as saturation, efficiency changes, and nonlinear responses.* $\left(\frac{d}{dt}P_{net}(t)\right)^2$ *and* $\left(\frac{d}{dt}SoC(t)\right)^2$ *enhance stability by damping oscillations and transients. In the fuzzy framework, these terms reinforce inferential capacity by emphasizing memory and critical states, ensuring effective responses even in extreme conditions.*

Remark 3 $\mu(P_{net}(t))$ *and* $\mu(SoC(t))$ *are made dimensionless via two steps: (i) normalize PID terms by their theoretical maxima; (ii) apply a global rescaling to ensure numerical consistency, cross-variable compatibility, and computational stability. The resulting dimensionless functions are directly comparable within the fuzzy framework, enabling coherent handling of heterogeneous variables and stable control under disturbances or rapid changes, while remaining adaptable through tunable normalization parameters.*

7 Adaptive parameter tuning

The output power $P_{PV}(t)$ in (1) depends on $G_t(t)$ and $T_{amb}(t)$, introducing significant temporal variability. This dynamic behavior requires a control system capable of continuous adaptation. $P_{mechanical}(t)$ in (2) is a function of $(v(t))^3$, further amplifying the variability. To ensure effective normalization, the maximum net power is dynamically updated as $P_{\max} = \mathrm{percentile}_{95}(|P_{\mathrm{net}}(t)|)$, along with its maximum derivative. As for the battery, $\%SoC(t)$ is described by (3), with its maximum derivative defined as:

$$\dot{SoC}_{\max} = \max_t \left| \frac{dSoC(t)}{dt} \right|. \tag{25}$$

The parameters are uniformly initialized using

$$\alpha_0' = k_\alpha' = \beta_0' = k_\beta' = \gamma_0' = k_\gamma' = \frac{1}{N_P}, \tag{26}$$
$$\lambda_0' = k_\lambda' = \delta_0' = k_\delta' = \eta_0' = k_\eta' = \frac{1}{N}.$$

If the response time T_r exceeds the desired threshold ($T_r > 10\,\mathrm{s}$), the proportional terms are increased, $\beta_0' \leftarrow \beta_0' + \kappa_\beta \beta_0', \quad k_\beta' \leftarrow k_\beta' + \kappa_\beta k_\beta'$, with $\kappa_\beta \in [0.01, 0.1]$. If excessive oscillations are observed, the derivative terms are reduced, $\gamma_0' \leftarrow \rho\gamma_0', \quad k_\gamma' \leftarrow \rho k_\gamma'$, with $\rho = 0.7$. In the case of significant steady-state error, the integral terms are increased, $\alpha_0' \leftarrow \alpha_0' + \kappa_\alpha \alpha_0', \quad k_\alpha' \leftarrow k_\alpha' + \kappa_\alpha k_\alpha'$, with $\kappa_\alpha \in [0.03, 0.05]$. The parameter adaptation in $\mu(\mathrm{SoC}(t))$ follows the same logic, modifying the weights λ', δ', η' according to the speed and regularity of the state of charge response. Since fuzzy functions are defined within the interval $[0, 1]$, stability cannot be assessed based on absolute bounds of the response, but it is analyzed in terms of signal regularity. A function is considered stable if, following a disturbance, its oscillations decrease over time and it shows no discontinuous jumps. More formally, stability is verified by checking that $|\mu(t_{n+1}) - \mu(t_n)| < |\mu(t_n) - \mu(t_{n-1})|$ for consecutive time instants $t_{n+1} > t_n > t_{n-1}$. The procedure is considered complete when the following criteria are satisfied:

$$T_r \leq 10\,\mathrm{sec}, \quad |\mu(P_{\mathrm{net}}(t)) - \mu_{\mathrm{target}}| < \varepsilon, \tag{27}$$
$$|\mu(SoC(t)) - \mu_{\mathrm{target}}| < \varepsilon, \quad \varepsilon \approx 0.01.$$

This strategy enables the EMS to exhibit smooth, predictable, and responsive behavior, ensuring efficient energy balancing, resource protection, and uninterrupted power supply even under changing operating conditions.

8 Simulation scenario

The developed EMS was implemented in the MatLab Simulink R2023a simulation environment, with the aim of evaluating the performance of the fuzzy PID-inspired controller under realistic yet simulated operating conditions. The case study refers to the DICEAM Department of the University "Mediterranea" of Reggio Calabria (coordinates: 38° 7' 15.138" N / 15° 39' 55.315" E), located on the Strait of Messina. Since academic activities pause for only twenty days in August, July 20th, 2023, was selected for simulation. The simulation horizon is 24 hours, with a time step $\Delta t = 1$ s, used for both dynamic model integration and fuzzy rule updates within the EMS. Operating and environmental conditions are defined through synthetic data generated to represent a Mediterranean summer profile, characterized by significant irradiance and temperature variations (see Fig. 2). Photovoltaic power is computed using model (1), assuming $\alpha_t = -3.7 \times 10^{-3}$ °C^{-1}. The irradiance profile $G_t(t)$ reaches a peak of $1000\,\mathrm{W\,m^{-2}}$ during midday and approaches zero at night. Ambient temperature $T_{\mathrm{amb}}(t)$ varies between 20 °C and 30 °C, following a sinusoidal daily trend. Wind power is obtained through the classical aerodynamic model (2), where $\rho = 1.225\,\mathrm{kg\,m^{-3}}$ is air density and R is the blade radius, typical of a residential or commercial turbine. The wind speed profile $v(t)$ is generated using a Weibull distribution with parameters $k = 2$ and $c = 7\,\mathrm{m\,s^{-1}}$, to introduce intraday variability into the wind model. The battery is modeled through the integral energy balance equation (3), with operational constraints defined between $\mathrm{SoC}_{\mathrm{min}} = 20\%$ and $\mathrm{SoC}_{\mathrm{max}} = 80\%$, and an initial condition of $SoC(0) = 50\%$. The fuel cell is modeled as a controlled generator with output power ranging from 0 to 10 kW, activated based on the fuzzy rules inferred by the control system. The load profile $P_{\mathrm{load}}(t)$ is designed to include two main peaks, one in the morning and another in the evening, along with a base level during nighttime hours (see Figs. 3a and (3b)). This allows assessment of the EMS's ability to respond dynamically and robustly to both energy surplus and deficit conditions. All signals used in the simulation are synthetically generated, without reliance on real time series, to ensure full control over operating conditions and critical system variables.

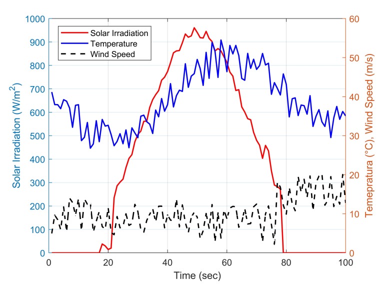

Figure 2: Solar irradiation (W/m²), temperature (°C), wind speed (m/s) at the selected location on July 20, 2023 (simulated data).

The range of the fuzzy bracket depends on both the numerator, $\mu(P_{\mathrm{net}}(t)) - \mu(\mathrm{SoC}(t))$, and the denominator, $1 + |\mu(P_{\mathrm{net}}(t))| + |\mu(\mathrm{SoC}(t))|$. When the fuzzy variables $\mu(P_{\mathrm{net}}(t))$ and $\mu(\mathrm{SoC}(t))$ are normalized within the inter-

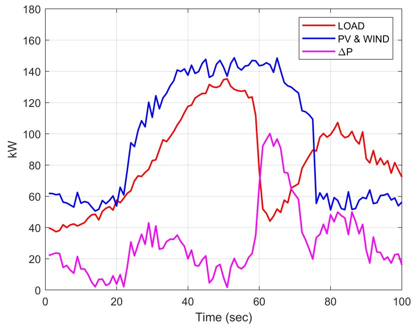

(a) Simulated power evolution of load side and PV/WT (simulated data).

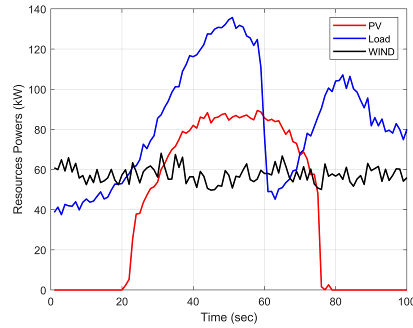

(b) Power profile of the load, PV/WT generation (simulated data).

Figure 3: RES and Load Profiles (Simulated Data).

val $[0, 1]$, the numerator ranges from -1 to 1, while the denominator takes values between 1 and 3. Consequently, the fuzzy bracket lies within the interval:

$$-\frac{1}{3} \leq [\mu(P_{\text{net}}(t)), \mu(\text{SoC}(t))]_\mu \leq \frac{1}{3}. \tag{28}$$

To facilitate the interpretation of its value, the theoretical interval of the bracket is divided into four sub-intervals, as shown in Table 1.

Table 1: Partitioning of the bracket numerical range.

Label	**Range**
Low (L)	$L = \left[-\frac{1}{3}, -\frac{1}{9}\right)$ indicates an energy surplus, with $\mu(P_{\text{net}}(t))$ significantly lower than $\mu(\text{SoC}(t))$.
Medium (M)	$M = \left[-\frac{1}{9}, \frac{1}{9}\right]$ represents a condition of relative balance between demand and generation.
High (H)	$H = \left(\frac{1}{9}, \frac{1}{3}\right]$ indicates an energy deficit, with $\mu(P_{\text{net}}(t))$ significantly greater than $\mu(\text{SoC}(t))$.
Equilibrium (E)	$E = [-\epsilon, \epsilon]$, with $\epsilon = 0.01$, defines an almost perfect balance between demand and generation.

Regarding $P_{FC}(t)$, we start from the fact that its technical specifications require $P_{\min} = 0\,\text{kW}$ and $P_{\max} = 10\,\text{kW}$. We then divide the range $(P_{\min}, P_{\max}]$ into sub-intervals, as shown in Table 2, to define the possible value ranges for $P_{FC}(t)$.

Remark 4 *Partitioning the fuel cell power into five linguistic levels (Off – High) implements a pragmatic control that balances responsiveness and effi-*

Table 2: Partitioning of the numerical range of $P_{FC}(t)$.

Label	**Range**	**Label**	**Range**
Off	$P_{FC}(t) = 0$	**Minimum**	$P_{\min} < P_{FC}(t) \leq 0.2P_{\max}$
Low	$0.2P_{\max} < P_{FC}(t) \leq 0.4P_{\max}$	**Medium**	$0.4P_{\max} < P_{FC}(t) \leq 0.7P_{\max}$
High	$0.7P_{\max} < P_{FC}(t) \leq P_{\max}$		

ciency. Thresholds at 20%, 40%, and 70% of rated power capture nonlinear behavior and avoid suboptimal operation, reducing hydrogen use and wear. This granularity makes the fuzzy inference more interpretable and ensures smooth transitions between operating states.

Once the operating limits for $P_{FC}(t)$ are defined, we propose the partitioning for $\%SoC$ as outlined in Tab. 3.

Table 3: Partitioning of the numerical range of $\%SoC$

Label	**Range**
Low	$SoC \leq SoC_{\min} + 0.2(SoC_{\max} - SoC_{\min}) \Rightarrow 0 \leq \mu(SoC(t)) \leq 0.3.$
Medium	$SoC_{\min} + 0.2 \cdot (SoC_{\max} - SoC_{\min}) < SoC \leq SoC_{\min} + 0.7(SoC_{\max} - SoC_{\min}) \Rightarrow 0.3 < \mu(SoC(t)) \leq 0.7$
High	$SoC > SoC_{\min} + 0.7(SoC_{\max} - SoC_{\min}) \Rightarrow 0.7 < \mu(SoC(t)) \leq 1$

Remark 5 *The partitioning of the $\%SoC$ domain into Low, Medium, and High intervals is designed to reflect the operational status of the battery with respect to its technical limits. The threshold at 20% above the minimum allows early detection of critical discharge conditions, while the 70% threshold below the maximum marks an efficient storage level. This segmentation enables the fuzzy system to provide a more responsive and context-aware control action in the most relevant operational zones.*

9 Complete set of fuzzy rules

This section introduces the complete fuzzy rule base that determines the FC set-point. The rules are organized into four operating situations—deficit, surplus, near-balance, and transitional/emergency conditions—and map the previously defined domain partitions to FC intervention levels, while respecting device constraints.

9.1 Rules for energy deficit

Table 4 summarizes the fuzzy rules used for energy deficit management. Operating conditions are classified based on the imbalance level between demand and generation, expressed by the value of $[\mu(P_{\text{net}}(t)), \mu(\text{SoC}(t))]_\mu$, and by $\mu(\text{SoC}(t))$. When the deficit is high and the battery is nearly discharged, $P_{FC}(t)$ is required to provide maximum support to ensure power continuity. Conversely, if the battery is sufficiently charged, the EMS reduces the fuel cell output, balancing the use of both resources. For moderate deficits, the fuel cell's contribution ranges from medium to high depending on the state of charge, while in low-deficit conditions, the battery supplies most of the demand, minimizing fuel cell activation. These rules enable optimized combined use of energy resources, preserving battery life and reducing fuel consumption.

Table 4: Fuzzy rules for energy deficit management

Scenario	**Condition and Action**
High deficit, battery nearly discharged	Condition: $[\mu(P_{\text{net}}(t)), \mu(\text{SoC}(t))]_\mu$ is *H*. Rule: IF $[\mu(P_{\text{net}}(t)), \mu(\text{SoC}(t))]_\mu$ is *H*, THEN $P_{FC}(t)$ is *H*. Action: Significantly increase P_{FC}.
High deficit, battery fully charged	Condition: $[\mu(P_{\text{net}}(t)), \mu(\text{SoC}(t))]_\mu$ is *H*, and $\mu(\text{SoC}(t))$ is *M*. Rule: IF $[\mu(P_{\text{net}}(t)), \mu(\text{SoC}(t))]_\mu$ is *H*, THEN $P_{FC}(t)$ is *M*. Action: Balance the use of the FC and the battery.
Moderate deficit, battery nearly discharged	Condition: $[\mu(P_{\text{net}}(t)), \mu(\text{SoC}(t))]_\mu$ is *M*, and $\mu(\text{SoC}(t))$ is LOW. Rule: IF $[\mu(P_{\text{net}}(t)), \mu(\text{SoC}(t))]_\mu$ is *M*, THEN $P_{FC}(t)$ is *H*. Action: Increase the intervention of the fuel cell.
Moderate deficit, battery charged	Condition: $[\mu(P_{\text{net}}(t)), \mu(\text{SoC}(t))]_\mu$ is *M*. Rule: IF $[\mu(P_{\text{net}}(t)), \mu(\text{SoC}(t))]_\mu$ is *M*, THEN $P_{FC}(t)$ is *M*. Action: Balance the intervention between the battery and the fuel cell.
Low deficit, battery charged	Condition: $[\mu(P_{\text{net}}(t)), \mu(\text{SoC}(t))]_\mu$ is *L*. Rule: IF $[\mu(P_{\text{net}}(t)), \mu(\text{SoC}(t))]_\mu$ is *L*, THEN $P_{FC}(t)$ is *L*. Action: Manage the deficit primarily with the battery.

9.2 Rules for energy surplus

Tab. 5 summarizes the fuzzy rules adopted for managing the energy surplus within the microgrid. In the presence of a high surplus and a nearly full battery, the EMS turns off the FC ($P_{FC}(t) = \text{Off}$) and redistributes the excess energy to avoid overloads. When the surplus is moderate and the battery is already charged, the fuel cell power is reduced ($P_{FC}(t) = \text{L}$) to favor energy storage. In the case of a low surplus with a discharged battery, the system fully exploits the available surplus to recharge the battery, keeping the fuel cell at a minimum level ($P_{FC}(t) = \text{M}$). This fuzzy logic allows for optimized use of available resources, prevents battery overloads, and improves overall efficiency.

Table 5: Fuzzy rules for energy surplus management

Scenario	Condition and Action
High surplus, battery nearly full Rule: IF $[\mu(P_{\text{net}}(t)), \mu(\text{SoC}(t))]_\mu$ is *H*, THEN $P_{FC}(t)$ is *Off*. Action: Deactivate the fuel cell and redistribute the excess energy.	Condition: $[\mu(P_{\text{net}}(t)), \mu(\text{SoC}(t))]_\mu$ is *Alto*.
Moderate surplus, battery charged Rule: IF $[\mu(P_{\text{net}}(t)), \mu(\text{SoC}(t))]_\mu$ is *M*, THEN $P_{FC}(t)$ is *L*. Action: Use the surplus to charge the battery and reduce the fuel cell power.	Condition: $[\mu(P_{\text{net}}(t)), \mu(\text{SoC}(t))]_\mu$ is *M*.
Low surplus, battery discharged Rule: IF $[\mu(P_{\text{net}}(t)), \mu(\text{SoC}(t))]_\mu$ is *B*, THEN $P_{FC}(t)$ is *M*. Action: Use the surplus to fully charge the battery.	Condition: $[\mu(P_{\text{net}}(t)), \mu(\text{SoC}(t))]_\mu$ is *L*.

9.3 Rules for energy balance

Table 6 summarizes the fuzzy rules adopted for managing energy balance under conditions where the net power is close to zero ($P_{\text{net}} \approx 0$). Control actions on $P_{FC}(t)$ depend on $\mu(\text{SoC}(t))$, which distinguishes between a fully charged, moderately charged, or discharged battery. When the battery is fully charged, the fuel cell remains off, as no energy compensation is needed. With an intermediate charge level, the EMS maintains a minimal fuel cell contribution to compensate for small fluctuations in the energy balance. Finally, if the battery is discharged, the fuel cell is activated at a low level to allow partial recharging of the storage and to ensure a safety margin.

Table 6: Fuzzy rules for energy balance management

Scenario	**Condition and Action**
Balance with full battery	Condition: $\mu(P_{\text{net}}(t)) \approx 0$ and $\mu(\text{SoC}(t))$ is H. Rule: IF $P_{\text{net}} \approx 0$ and $\mu(\text{SoC}(t))$ is H, THEN $P_{FC}(t)$ is *Off*. Action: Keep the fuel cell turned off.
Balance with moderately charged battery	Condition: $\mu(P_{\text{net}}(t)) \approx 0$ and $\mu(\text{SoC}(t))$ is M. Rule: IF $P_{\text{net}} \approx 0$ and $\mu(\text{SoC}(t))$ is M, THEN $P_{FC}(t)$ is M. Action: Maintain balance through minimal intervention of the fuel cell.
Balance with discharged battery	Condition: $\mu(P_{\text{net}}(t)) \approx 0$ and $\mu(\text{SoC}(t))$ is L. Rule: IF $P_{\text{net}} \approx 0$ and $\mu(\text{SoC}(t))$ is L, THEN $P_{FC}(t)$ is L. Action: Allow the battery to recharge partially.

9.4 Rules for transition or emergency conditions

Tab. 7 presents the fuzzy rules defined for managing transition or emergency conditions. In particular, it considers the case when the battery is non-operational ($\mu(\text{SoC}(t)) = 0$), a situation that may occur due to faults or maintenance. In this scenario, the EMS assigns a high ($P_{FC}(t)$) to ensure continuity of supply and balance between demand and generation.

Table 7: Fuzzy rules for transition or emergency conditions

Scenario	**Condition and action**
Deficit or surplus with non-operational battery	Condition: $\mu(\text{SoC}(t)) = 0$ (battery not operational). Rule: IF $\mu(\text{SoC}(t)) = 0$, THEN $P_{FC}(t)$ is H. Action: rely entirely on the fuel cell to balance the system.

10 Bracket & Mamdani fuzzy inference system

This section describes how the fuzzy bracket is integrated into a Mamdani inference system to generate the FC power reference. It illustrates the input signals, the structure of the rule base, and the fuzzification and defuzzification steps that modulate the output as a function of energy surpluses or deficits.

10.1 Inputs-output and fuzzification

The proposed fuzzy system has two main inputs: the fuzzy bracket, denoted by $x_1(t) \in \left[-\frac{1}{3}, \frac{1}{3}\right]$, and $x_2(t) = \mu(\mathrm{SoC}(t)) \in [0, 1]$, the fuzzy battery state of charge. The system output is $y(t) = P_{FC}(t) \in [0, P_{\max}]$. Let $\mathcal{X}_1, \mathcal{X}_2$ be the input domains, and $\mathcal{Y}$ the output domain. The linguistic labels for $x_1(t)$ are $\mathcal{L}_1 = \{B, M, A, E\}$, while those for $x_2(t)$ are $\mathcal{L}_2 = \{\mathrm{Low}, \mathrm{Medium}, \mathrm{High}\}$. Finally, the output labels $y(t)$ are $\mathcal{L}_3 = \{\mathrm{Off}, \mathrm{Minimum}, \mathrm{Low}, \mathrm{Medium}, \mathrm{High}\}$. The membership functions associated with the linguistic subsets of the respective variables are defined as $\mu^{(1)}_{L_1^j}(x_1)$, $j = 1, \ldots, N_1$; $\mu^{(2)}_{L_2^k}(x_2)$, $k = 1, \ldots, N_2$; and $\mu^{(3)}_{L_3^r}(y)$, $r = 1, \ldots, N_3$, where L_1^j, L_2^k, L_3^r represent the labels associated, respectively, with x_1, x_2 and y; $\mu^{(i)}_{L_i^\ell}(\cdot)$ is the membership function of the linguistic set L_i^ℓ for variable x_i or y; and N_1, N_2, N_3 indicates the total number of linguistic sets used for each variable. The instantaneous fuzzification of the inputs consists in computing the overall activation degree of the linguistic sets associated with each input. Specifically, for each instant t, we have $\mu_{x_1}(x_1(t)) = \sum_{j=1}^{N_1} \mu^{(1)}_{L_1^j}(x_1(t))$, $\mu_{x_2}(x_2(t)) = \sum_{k=1}^{N_2} \mu^{(2)}_{L_2^k}(x_2(t))$ which represent the overall degree to which the inputs $x_1(t)$ and $x_2(t)$ satisfy the predefined linguistic conditions.

10.2 Fuzzy rule bank

Each rule of the fuzzy system has the following canonical structure:

$$R_{jk} : \text{IF } x_1 \text{ is } L_1^j \text{ AND } x_2 \text{ IS } L_2^k \text{ THEN } y \text{ è } L_3^{r(j,k)}, \tag{29}$$

where $j = 1, \ldots, N_1$, $k = 1, \ldots, N_2$, and $r(j,k) \in \{1, \ldots, N_3\}$. The linguistic labels L_1^j, L_2^k, and L_3^r represent the fuzzy subsets associated with the inputs x_1, x_2, and the output y, respectively. In addition to the standard rules, the following special operating conditions are considered to handle the system's boundary behaviors:

$$\text{IF } \mu(\mathrm{SoC}(t)) = 0 \quad \Rightarrow \quad P_{\mathrm{FC}}(t) = \mathrm{H}, \tag{30}$$

$$\text{IF } |x_1(t)| < \epsilon \Rightarrow \begin{cases} \mu(\mathrm{SoC}(t)) = \mathrm{L} \Rightarrow P_{\mathrm{FC}}(t) = \mathrm{L}, \\ \mu(\mathrm{SoC}(t)) = \mathrm{M} \Rightarrow P_{\mathrm{FC}}(t) = \mathrm{M}, \\ \mu(\mathrm{SoC}(t)) = \mathrm{H} \Rightarrow P_{\mathrm{FC}}(t) = \mathrm{Off}. \end{cases} \tag{31}$$

The activation degree of each fuzzy rule R_{jk}, which links the linguistic subsets L_1^j and L_2^k to the inputs x_1 and x_2, is determined through a conjunctive t-norm of the minimum type. At each time instant t, the activation is defined as the minimum of the respective membership function values:

$$\alpha_{jk}(t) = \min\left(\mu^{(1)}_{L_1^j}(x_1(t)),\ \mu^{(2)}_{L_2^k}(x_2(t))\right) \tag{32}$$

where $\mu^{(1)}_{L_1^j}$ and $\mu^{(2)}_{L_2^k}$ represent the membership degrees of the inputs $x_1(t)$ and $x_2(t)$ to the predefined linguistic sets. The obtained value represents the strength with which the rule R_{jk} is activated, based on the current conditions of the system. The aggregation of the contributions of the active rules is performed by combining the partial outputs, each defined as the minimum between the rule activation degree and the membership function associated with the output. The overall result is an aggregated fuzzy function, obtained via a max operator over all contributions:

$$\mu_{\mathrm{agg}}(y) = \max_{j,k}\left[\min\left(\alpha_{jk}(t),\ \mu^{(3)}_{L_3^{r(j,k)}}(y)\right)\right] \tag{33}$$

This aggregated function represents the overall degree to which the output y belongs to the fuzzy sets inferred by the rule base, in response to the instantaneous input values. The crisp output is finally computed via defuzzification using the discrete centroid method. In this case, the output universe is discretized into a finite number of points y_i, with $i = 1, \ldots, N$, and the final value of the power assigned to the fuel cell is given by:

$$P_{FC}(t) = \frac{\sum_{i=1}^{N} y_i \cdot \mu_{\mathrm{agg}}(y_i)}{\sum_{i=1}^{N} \mu_{\mathrm{agg}}(y_i)}. \tag{34}$$

Remark 6 *Integrating the fuzzy bracket into the PID adds negligible cost—just simple scalar arithmetic —while structurally modulating error signals to boost adaptability and robustness without extra complexity, enabling real-time embedded use and preserving the classical PID's simplicity and performance.*

Remark 7 *In some cases, special rules depend on a single input (e.g., $\mu(SoC(t)) = 0$ under extreme battery states), so they fall outside the bivariate form in* (29)*. For uniform inference, the missing antecedent is assigned membership zero, making $\alpha_{jk}(t) = 0$ unless explicitly treated as an exception. This preserves compatibility with max–min aggregation and overall mathematical consistency.*

11 Characteristics of RES and load profile based on real data

Referring to the case study described in Section 8, the real data used here were provided by the Technical Physics research group of the DICEAM Department at the University "Mediterranea". These data were collected using measurement units installed on-site and show solar radiation exceeding 900 W/m^2 and temperatures above 40 °C during the central hours of the day. The wind speed, also significant, indicates a good potential for energy production (see Fig. 4). These data were used for training the fuzzy system; a second real dataset with similar characteristics was used for the testing phase.

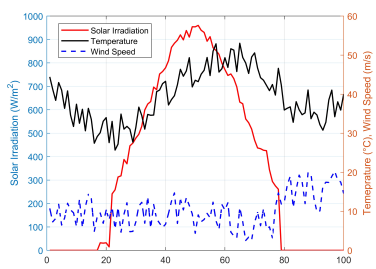

Figure 4: Solar irradiation (W/m^2), temperature (°C), and wind speed (m/s) recorded at the selected location on July 20, 2023 (real data).

The real load data, provided by the energy operator, along with renewable source data, were used for both training and testing. As shown in Fig. 5a, energy consumption is low in the early morning and early afternoon, corresponding to the suspension of teaching activities and cafeteria services. The peak demand, exceeding 135 kW, occurs around 1:30 PM. In the evening, consumption rises again due to a student-organized event and continues into the night. Photovoltaic production reaches a maximum slightly above 89 kW, which is lower than the load peak, and drops quickly in the afternoon as solar radiation decreases. Wind power production, varying between 49 kW and 67 kW, shows an evening increase due to the sea breeze.

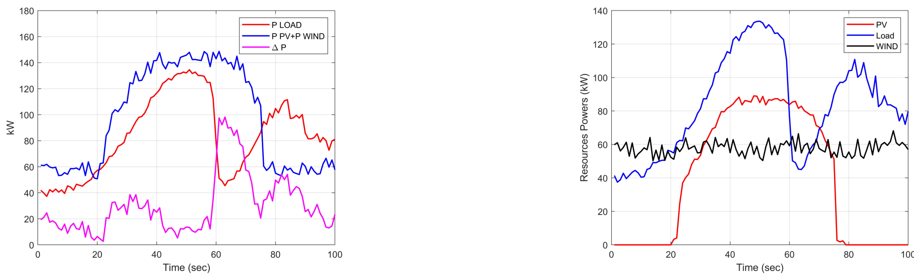

(a) Real power evolution of load side and PV/WT.

(b) Power profile of the load and PV/WT.

Figure 5: RES and Load Profiles (Real Data).

As shown in Fig. 5b, the generated power exceeds the demanded power until 5:00 AM and again from 5:30 AM to 6:00 PM. Afterwards, the increase in load and the reduction in photovoltaic generation result in a deficit. A second database of real data with consistent characteristics was also prepared for this analysis to validate the EMS.

12 Some relevant results

Fig. 6 presents a direct comparison between the EMS performance in two different scenarios: a simulated one (Fig. 6a) and a real one (Fig. 6b).Both plots show the time-varying power balance and each component's contribution to the load. The two scenarios behave almost identically—in response time and intervention intensity—with the fuel cell (red) consistently below the battery (blue). Thus, the battery alone meets the demand under the tested loads, implying minimal hydrogen use; the EMS preserves the fuel cell, activating it only in genuinely critical or sustained deficits. Quantitatively, the fuel-cell power traces yield a Pearson correlation $\rho > 0.95$, confirming strong temporal and dynamic consistency. Moreover, the mean absolute error (MAE) between the two fuel cell power profiles was found to be less than 5% of the average value, confirming that the EMS behaves similarly even in the presence of noise or disturbances in real data. Another noteworthy aspect is the presence of the power absorbed by the damp load, which is also visible in the plots. As the results show, the activation of the damp load does not negatively interfere with the EMS decisions. This is possible because the fuzzy controller considers only the net available power and the state of charge, assigning the damp load a passive and emergency role. It is triggered only under extreme conditions and does not influence the primary decision logic, which remains effective and consistent even in its presence.

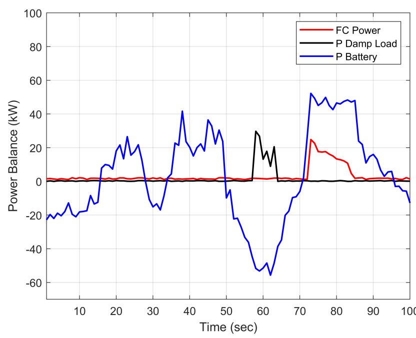

(a) Power balance for simulated data.

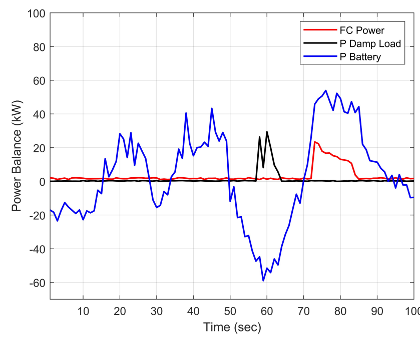

(b) Power balance for real data.

Figure 6: Comparison between results from simulated data and those obtained from real data.

Fig. 6 compares the EMS performance in two scenarios: a simulated one (Fig. 6a) and a real one (Fig. 6b). In both cases, the plots show the power balance over time, highlighting how the sources contribute to covering the electrical load. The system behavior is very similar in terms of response times and intervention intensity. The red curve, representing the power supplied by the FC, always remains below the blue curve, which corresponds to the battery, in both scenarios. This indicates that the battery can meet the energy demand with minimal use of the FC, resulting in negligible hydrogen consumption. This confirms that the EMS activates the FC only when strictly necessary, helping to preserve its operational lifespan. The consistency of the profiles is confirmed by a Pearson correlation coefficient greater than 0.95 and a MAE lower than 5% of the average power, even in the presence of noise or disturbances in the real data. Both scenarios include the intervention of the damp load, whose role is purely passive. The EMS, relying solely on net power and $\%SoC$, is not affected by its activation, which occurs only under extreme conditions and does not compromise control quality. Fig. 7 shows the battery state of charge trend, highlighting that in the real case, the $\%SoC$ is on average higher than in the simulation. Driven by slightly higher renewable output in the real data, more frequent short peaks at low load, and reduced FC usage that preserves charge, the real case shows a more active damp load absorbing surplus without affecting the control logic—indicating a favorable energy balance. The two $\%SoC$ curves differ by an almost constant vertical offset rather than an error; this systematic shift does not undermine the model's validity but simply reflects more favorable operating conditions under the same control strategy.

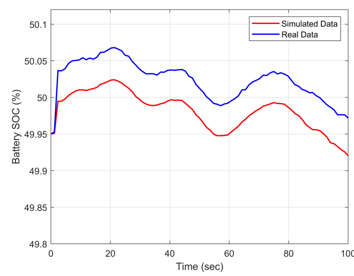

Figure 7: Temporal evolution of $\%SoC$: comparison between simulation and empirical data.

13 Conclusions and perspectives

This work introduces a fuzzy energy management strategy for stand-alone DC microgrids that uses a bracket operator to combine $P_{\text{net}}(t)$ and $\text{SoC}(t)$, resulting in a consistent, balanced and responsive controller with a simple, adaptive, real-time structure under uncertainty. Tests on simulated and real profiles show nearly identical behavior, with minimal deviations and a steady %SoC drift that does not affect system dynamics, confirming simulation as an effective design aid that reduces sizing errors. The damp load acts as a passive stabilizer without interfering with the fuzzy logic, and the method is easily implementable, extendable to hybrid AC/DC or grid-connected microgrids, and compatible with ML-based predictive techniques; implementation maps variables to normalized fuzzy sets, computes the bracket via a simple formula, and runs on microcontrollers or FPGAs to coordinate resources stably. Validation so far covers a single site over a summer month with high RES variability, with further studies (including extreme surplus conditions) underway; the fuzzy-PID remains far lighter than AI controllers (U-Net, LSTM), and performance can be further improved through metaheuristic or multi-objective optimization to refine calibration and adapt fuzzy rules to diverse scenarios.

Acknowledgements. Paper written with the support of: the Italian National Group of Mathematical Physics (GNFM-INdAM) and the University of Messina through FFABR-UNIME 2023; the Next Generation EU-Italian NRRP, Mission 4, Component 2, Investment 1.5, call for the creation and strengthening of 'Innovation Ecosystems', building 'Territorial R&D Leaders' (Directorial Decree n. 2021/3277)–project Tech4You– Technologies for climate change adaptation and quality of life improvement, n. ECS0000009 (in particular, action 9 of Spoke 2—Goal 2.1—Pilot Project 1; 2).

References

[1] G. Angiulli, A. Jannelli, F.C. Morabito and M. Versaci, Reconstructing the membrane detection of a 1 D electrostatic-driven MEMS device by the shooting method: convergence analysis and ghost solutions identification, *Comput. Appl. Math.* 37 (2018), 4484-4498.

[2] A. Belqasem et al., Optimization of DC, AC, and hybrid AC/DC microgrid-based IoT systems: a review, *Energies* 15 (2022), 6813.

[3] L. Bonaccorsi, R. Carbone, F. La Foresta, C. Marinom, A. Nucara, M. Pietrafesa and M. Versaci, Operational analysis of a pilot-scale plant for hydrogen production via an electrolyser powered by a photovoltaic system, *Energies* 18 (2025), 3949.

[4] C. Chiu and Y. Ouyang, Robust maximum power tracking control of uncertain photovoltaic system: a unified T-S fuzzy model-based approach, *IEEE Trans. Control Syst. Technol.* 19 (2011), 1516-1526.

[5] A. Dabiri, B.P Moghaddam and J.T. Machado, Optimal variable-order fractional PID controllers for dynamical systems, *J. Comput. Appl. Math.* 339 (2018), 40-48.

[6] A. Dev et al., Advancements and challenges in microgrid technology: a comprehensive teview of control strategies, emerging technologies, and future directions, *Energy Sci. Eng.* 13 (2025), 2112-2134.

[7] A. El Zerk and M. Ouassaid, Real-time fuzzy logic based energy management system for microgrid using hardware in the loop, *Energies* 16 (2023), 2244.

[8] O. Husev, Oleksandr and D Vinnikov, DC microgrid: State of art, driving force, challenges and perspectives, *Power Systems Research and Operation: Selected Problems III* (2023), 149-190.

[9] K.S. Joshal and N. Gupta, Microgrids with model predictive control: A critical review, *Energies* 16 (2023), 4851.

[10] A.M. Mohamed, M. Hassanin and A. Hassan, Optimization of stand-alone hybrid renewable energy systems using different metaheuristic techniques considering demand side management, *J. Adv. Eng. Trends* 44 (2025), 159-186.

[11] F.C. Morabito, Independent component analysis and feature extraction techniques for NDT data, *Mater. Eval.* 58 (2000), 85–92.

[12] A. Ouacel, B. M'Hamdi, T. Benaissa, A. Amari, M. Pietrafesa and M. Versaci, Maximum power point tracking based on improved sliding mode control, *The European Phys. J. Plus* 140 (2025), 1-18.

[13] A.K. Rajput and S.L. Jagdeep, Adaptive energy management strategy for a DC microgrid using intelligent Controller, *Smart Sci.* 13 (2025), 77-93.

[14] G. Simone, F.C. Morabito, R. Polikar, P. Ramuhalli, L. Udpa and S. Udpa, Feature extraction techniques for ultrasonic signal classification, *Int. J. Appl. Electromagn. Mech.* 15 (2002), 291-294.

[15] V. Subramanian, I. Vairavasundaram and B. Aljafari, Analysis of optimal load management using a stand-alone hybrid AC/DC microgrid system *Int. Trans. Elect. Energy Syst.* 2023 (2025), 7519436.

[16] M. Versaci and F. La Foresta, Fuzzy approach for managing renewable energy flows for DC-microgrid with composite PV-WT generators and energy storage system, *Energies* 17 (2024), 402.

[17] M. Versaci, F. La Foresta, F. Laganà and F.C. Morabito, Stand-alone DC-MSs & TS fuzzy systems for regenerative urban design, *Lect. Notes Networks Syst.* (2024), Springer, Cham.

[18] N. Zemouri, Z. Zemali, F. La Foresta, M. Versaci and G. Angiulli, Hybrid AI-Based framework for renewable energy forecasting: one-stage decomposition and sample entropy reconstruction with least-squares regression, *Energies* 18 (2025), 1-40.

[19] Z. Zhong, *Modeling, Control, Estimation, and Optimization for Microgrids - A Fuzzy-Model-Based Method*, CRC Press, Taylor & Francis Group, 2023.